

## Article

# Efficient Removal of Rhodamine B in Wastewater via Activation of Persulfate by MnO<sub>2</sub> with Different Morphologies

Xinyi Zhang <sup>1,2</sup>, Xinrui Gan <sup>1</sup>, Shihu Cao <sup>1</sup>, Jiangwei Shang <sup>1,2</sup> and Xiuwen Cheng <sup>1,2,\*</sup>

<sup>1</sup> Key Laboratory of Pollutant Chemistry and Environmental Treatment, College of Chemistry and Environmental Science, Yili Normal University, Yining 835000, China

<sup>2</sup> Key Laboratory for Environmental Pollution Prediction and Control, College of Earth and Environmental Sciences, Lanzhou University, Lanzhou 730000, China

\* Correspondence: chengxw@lzu.edu.cn

**Abstract:** In recent years, typical organic pollutants were frequently found in aquatic environments. Among them, synthetic dyes were widely used in many industries, which resulting in a large amount of wastewater contained dyes. Because of the characteristic of complex components, poor biodegradability and high toxicity, this kind of wastewater brought lots of harm to the ecological environment and organism. In this study, three different types of manganese dioxide (MnO<sub>2</sub>) with the rod-like, needle-like and mixed morphologies respectively were successfully fabricated by hydrothermal method with changing the preparation conditions and addition of the metal ions, and utilized as activator of persulfate (PS) to remove the dyes aqueous. Subsequently, these MnO<sub>2</sub> nanocomposite was characterized by X-ray diffraction (XRD) and scanning electron microscope (SEM) measurements. In addition, Rhodamine B (Rh B), as a representative substance of xanthene dyes was chosen as the target degradants to researched and compared the efficiency of removal via PS activated by different MnO<sub>2</sub>. By exploring the influences of different reaction parameters on the result of removal, results indicated that PS activated by the acicular MnO<sub>2</sub> ( $\alpha$ -MnO<sub>2</sub>) can remove 97.41% of Rh B over 60 min, with the optimal catalyst/PS ratio of 2:1 (the concentration of the  $\alpha$ -MnO<sub>2</sub> and PS were 1.2 g/L and 0.6 g/L, respectively), pH value of 3, at the temperature of 20 °C. Meanwhile, the probable degradation mechanism was also proposed. At last, as the catalyst was reused for four times, the degradation rate of target degradants decreased less than 10%.

**Keywords:** PS; MnO<sub>2</sub>; morphologies; SO<sub>4</sub><sup>•-</sup>; mechanism



**Citation:** Zhang, X.; Gan, X.; Cao, S.; Shang, J.; Cheng, X. Efficient Removal of Rhodamine B in Wastewater via Activation of Persulfate by MnO<sub>2</sub> with Different Morphologies. *Water* **2023**, *15*, 735. <https://doi.org/10.3390/w15040735>

Academic Editors: Gassan Hodaifa, Antonio Zuorro, Joaquín R. Dominguez, Juan García Rodríguez, José A. Peres, Zacharias Frontistis and Mha Albqmi

Received: 25 December 2022

Revised: 2 February 2023

Accepted: 8 February 2023

Published: 13 February 2023



**Copyright:** © 2023 by the authors. Licensee MDPI, Basel, Switzerland. This article is an open access article distributed under the terms and conditions of the Creative Commons Attribution (CC BY) license (<https://creativecommons.org/licenses/by/4.0/>).

## 1. Introduction

In recent decades, with the rapid development of industrialization and urbanization, the environmental problems caused by refractory organic wastewater are becoming increasingly serious and need to be effectively treated [1]. Due to the widespread usage of synthetic dyes in printing, dyeing, papermaking, textile, cosmetics, leather and other industries [2], a large number of highly toxic, complex ingredients, and difficult to biodegradable dye wastewater have been produced, and many organic dyes are difficult to metabolize in the body, gradual accumulation causes great harm to human health and ecological environment [3]. Therefore, it is crucial to find a more efficient and green treatment method to degrade organic dye wastewater. The rhodamine series of dyes are 3',6' diaminated xanthene-like fluorescents with excellent pH stability and a variety of structures, and different structures offer fluorescence with different wavelengths and colors. Rhodamine B (Rh B), as a representative substance of xanthene dyes, is most common and most frequently used, similar to diphenylmethane and triphenylmethane derivatives, generally used in industries such as colored glass, paper, textiles, fireworks, and etc. It is difficult to degrade in the environment, highly toxic, persistent and carcinogenic [4]. Herein, Rh B was selected as target pollutants in this study. It is hoped to provide some methods and references for the degradation of such organic dyes.

The usual methods for treating dyeing and printing wastewater include physical, biological and chemical methods. The commonly used physical methods generally include: adsorption, coagulation, membrane treatment, reverse osmosis, ion exchange and etc. However, physical methods face many application limitations: (1) adsorption materials are not suitable for hydrophobic dyes, and the regeneration cost is high and the loss is large; (2) coagulation method is not effective for hydrophilic dyes, and it is easy to produce sludge that needs further treatment; (3) membrane treatment and reverse osmosis membrane can treat printing and dyeing wastewater well, but the cost is too high, the membrane is easy to clog, and the treatment and disposal of waste membrane is also a problem; (4) ion exchange method is only suitable for treating ionic dye wastewater, and it needs to be regenerated continuously, which results in high loss. In addition, the biological treatment method is not ideal for dye wastewater because most of these dyes are poorly biochemical and difficult to biodegrade, among which it has been confirmed that reactive dyes are the most difficult to be degraded in dyeing wastewater [5,6]. Chemical methods refer to the oxidation of organic pollutants using oxidants, and the commonly used oxidants are  $\text{H}_2\text{O}_2$ ,  $\text{NaClO}$ ,  $\text{O}_3$  and etc. The chemical method has the characteristics of good treatment effect, fast reaction rate, complete degradation of pollutants, high treatment efficiency and wide application range. Commonly used chemical methods are through the oxidant degradation of pollutants, and will use photocatalysis [7], electrocatalysis [8], high temperature and other means to catalyze the oxidant to produce a large number of hydroxyl radicals to improve the degradation effect. However, for some hard-to-degrade organic substances, traditional chemical methods still cannot effectively degrade them.

Advanced oxidation processes (AOPs), which have been developed in recent years, are currently attracting much attention and can make most organic pollutants to be effectively degraded by producing free radicals as the main active substance to eliminate pollutants completely [9]. It is mainly represented by AOPs based on sulfate radical ( $\text{SO}_4^{\bullet-}$ ) and hydroxyl radical ( $\bullet\text{OH}$ ). By contrast,  $\text{SO}_4^{\bullet-}$  possesses a higher redox potential than  $\bullet\text{OH}$  (redox potential of  $\bullet\text{OH}$  is 2.8 eV, while the  $\text{SO}_4^{\bullet-}$  is 2.5–3.1 eV) [10];  $\text{SO}_4^{\bullet-}$  has better selectivity through electron transfer, dehydrogenation, addition reaction to degrade organic matter [11];  $\text{SO}_4^{\bullet-}$  is more stable than  $\bullet\text{OH}$  due to its shorter half-life [12]; the way to produce  $\text{SO}_4^{\bullet-}$  is also easier and the origin of which shows a higher stability [13]. Currently, AOPs based on  $\text{SO}_4^{\bullet-}$  radicals generally generate  $\text{SO}_4^{\bullet-}$  radicals by activating persulfates, including peroxydisulfate (PS) and peroxymonosulfate (PMS). Among them, PS is a solid that exists stably at room temperature, is easily preserved for transport and transfer, dissolves easily in water, and is relatively inexpensive. The PS itself, as a strong oxidizing agent, can also produce  $\text{SO}_4^{\bullet-}$  radicals in aqueous solution without a catalyst. In general, PS is more stable and the above reaction rates are extremely low. After activation by applied energy or catalyst, the peroxygen bond (O-O bond) in the PS breaks and a large number of  $\text{SO}_4^{\bullet-}$  radicals can be efficiently produced with strong oxidizing properties. Herein,  $\text{SO}_4^{\bullet-}$  radicals can degrade difficult-to-treat organic pollutants in wastewater into biodegradable pollutants or even directly mineralize to carbon dioxide and water. In this process,  $\text{SO}_4^{\bullet-}$  radicals will be reduced to sulfate ( $\text{SO}_4^{2-}$ ), and no toxic and harmful substances will be produced, which is an environmentally friendly oxidant.

Therefore, the activation technology of PS has become the focus of current research. The most commonly used PS activation methods are thermal activation, ultrasound, photoactivation, and transition metal activation [14]. The reactions involved are as follows:



adjust the pH in the reaction parameter influence tests. All the experiments were carried out for three times to minimize the errors (2)



However, some of these methods require a large number of high-cost oxidants, high reaction conditions, or consume large amounts of energy [15]; likewise, some metal oxides or metal ions as catalysts are prone to secondary pollution, such as  $\text{Co}^{2+}$ ,  $\text{Co}_3\text{O}_4$ ,  $\text{CuO}$ , etc. [16–18]. Thus, the exploration and development of green and efficient persulfate activator has become a hot spot and focus now.

Manganese oxides are considered as common mineral oxides found in sediments and soils [19]. Among the various catalyst materials,  $\text{MnO}_2$  has become a very promising candidate because of its natural abundance, wide source, low cost, high activation, and low toxicity [20]. Because of its superior oxygen mobility, manganese oxides can induce a wider range of redox reactions [21]. More importantly, the reactivity of manganese-based oxides is relatively high. Meanwhile, as a promising alternative to iron minerals, manganese oxides are often applied in Fenton or Fenton-like reactions [22]. In recent reports,  $\text{MnO}_2$  have attracted considerable attention as activator for PS [23], especially, multi-component magnetic material compounded with it [19,24]. In this paper, three different morphologies of  $\text{MnO}_2$  activated PS were prepared to degrade organic pollutants, which can provide a certain reference for the technology of activation of PS with  $\text{MnO}_2$  and research of its multielement composite.

Herein, the main works of this study are: (1) Preparation of catalyst materials: three different morphologies of  $\text{MnO}_2$  were fabricated by hydrothermal method by changing the reaction conditions and adding metal ions; (2) Characterization of catalysts' crystallographic structure and micromorphology: X-ray diffraction (XRD) was employed to analyze the materials' composition and structure of atoms or molecules inside. Scanning electron microscope (SEM) was used to observe the microscopic surface morphology of the  $\text{MnO}_2$  with different morphologies; (3) Study on the catalytic performance: Rhodamine B was chosen as target pollutants to evaluate the catalytic activity of  $\text{MnO}_2$  on PS activation. The tests of exploring the influences of different reaction parameters on the result of removal were also conducted; (4) Stability evaluation: the repeated degradation experiments were carried out for 4 times. The main objective of this study was to compare and select the most dominant species among three different morphologies of  $\text{MnO}_2$  catalysts and to reveal the relationship between the microscopic morphology of the materials and their performance in activating PS for Rh B degradation. Ultimately, this research was expected to provide an important reference for the study of the activation of PS by  $\text{MnO}_2$  and their multicomponent complexes and the development of new nanomaterials for the efficient removal of organic dyes from wastewater.

## 2. Materials and Methods

### 2.1. Chemicals

Potassium permanganate ( $\text{KMnO}_4$ ), manganese sulfate monohydrate ( $\text{MnSO}_4 \cdot \text{H}_2\text{O}$ ), manganese chloride tetrahydrate ( $\text{MnCl}_2 \cdot 4\text{H}_2\text{O}$ ), ferric chloride hexahydrate ( $\text{FeCl}_3 \cdot 6\text{H}_2\text{O}$ ), potassium persulfate ( $\text{K}_2\text{S}_2\text{O}_8$ ), hydrochloric acid (HCl), absolute ethanol ( $\text{C}_2\text{H}_5\text{OH}$ ), sulfuric acid ( $\text{H}_2\text{SO}_4$ ), potassium hydroxide (KOH), Rhodamine B ( $\text{C}_{28}\text{H}_{31}\text{ClN}_2\text{O}_3$ , Rh B) were purchased from Kermel Chemical Reagent Co. Ltd. (Tianjin, China). All the chemicals above were directly used when received without further purification. Noted, deionized (DI) water was used throughout this experiment.

### 2.2. Fabrication of $\text{MnO}_2$ with Different Morphologies

In this experiment,  $\text{MnO}_2$  was prepared by hydrothermal method. By changing the preparation conditions, the reactant ratio and trying to add metal ions as auxiliary agents, three different morphologies of  $\text{MnO}_2$  were obtained.

#### 2.2.1. Fabrication of Rod-Shaped $\text{MnO}_2$

8 mmol (1.3520 g) of  $\text{MnSO}_4 \cdot \text{H}_2\text{O}$  and 8 mmol (1.2640 g) of  $\text{KMnO}_4$  dissolved in 50 mL of deionized water, and performed magnetic stirring for 30 min to dissolve fully. The mixed solution was then transferred to a 100 mL Teflon-lined stainless-steel autoclave,

sealed and kept at 140 °C for 12 h. After cooling to room temperature, the precipitate was centrifuged and washed with deionized water and absolute ethanol alternately three times, finally dried in a vacuum oven at 120 °C for 12 h. The sample was ground and stored for following use [25].

### 2.2.2. Fabrication of Acicular MnO<sub>2</sub>

The fabrication conditions of the above rod-shaped MnO<sub>2</sub> were changed to some extent, instead of changing the dosing ratio of MnSO<sub>4</sub>•H<sub>2</sub>O and KMnO<sub>4</sub> (1:1), an appropriate amount of iron ions (Fe<sup>3+</sup>) was added to the reaction system. In this test, 1 mmol (0.2702 g) of FeCl<sub>3</sub>•6H<sub>2</sub>O was added to the mixed solution, followed by magnetic stirring for 30 min to dissolve thoroughly. The mixed solution was then transferred to a 100 mL Teflon-lined stainless-steel autoclave, sealed and placed in a vacuum oven at 140 °C for 12 h. After cooling to room temperature, subsequent processing was consistent with the rod-shaped MnO<sub>2</sub> above. After grinding, sample was stored for use [26].

### 2.2.3. Fabrication of Mixed MnO<sub>2</sub>

To obtain the mixed MnO<sub>2</sub>, 1.5 mmol (0.2970 g) of MnCl<sub>2</sub>•4H<sub>2</sub>O and 2.5 mmol (0.3950 g) of KMnO<sub>4</sub> were dissolved in 50 mL of deionized water, and 0.45 mmol (0.1216 g) of FeCl<sub>3</sub>•6H<sub>2</sub>O were added to the mixture, which was sufficiently dissolved by vigorously stirring. The mixed solution was poured into a Teflon-lined stainless-steel autoclave, sealed and kept at 150 °C for 24 h. After cooling to room temperature, the treatment of the precipitate simulated the preparation process of the first two types of MnO<sub>2</sub> [27].

## 2.3. Characterizations

Powder X-ray diffraction (XRD) spectrograms of the samples were obtained on Panalytical multifunctional powder X-ray diffractometer (XRD D8 Advance, Rigaku Corporation, Matsumoto, Japan) with a graphite monochromatic Cu K $\alpha$  radiation ( $\lambda = 0.15418$  nm). The morphology and microstructure of three types of MnO<sub>2</sub> were determined by field-emission scanning electron microscopy (SEM, Japan Electron Optics Laboratory Co. Ltd., Mitaka, Tokyo, JSM-6701F) at 20 kV.

## 2.4. Catalytic Activity Tests

Prepared a 10 mg/L Rh B solution of the target substance for use and took 50 mL each time into 100 mL Erlenmeyer flasks, added a certain amount of catalyst and PS, then marked according to different reaction conditions. At the same time, set a blank group and pure adsorption group to contrast. Degradation experiments were conducted at the temperature of 20 °C, on the shaking table with the rocking speed kept 180 rpm. After the given time intervals, 5 mL of mixed solution was aspirated with a syringe and filtered through a 0.22  $\mu$ m to remove the catalyst, and immediately measured at maximum absorption wavelengths of the Rh B (549 nm) in a T6 UV-vis spectrophotometer (Evolution 300, Thermo Fisher Scientific Inc., Shanghai, China) [28]. Besides, the ratio of the measured absorbance of the sample to the absorbance of the initial target solution ( $A_t/A_0$ ) was regarded as the analysis index. Where  $A_t$  was the absorbance measured for each sampled sample and  $A_0$  was the absorbance of the initial 10 mg/L solution of the target pollutant. Meanwhile, in the following equation,  $C_0$  was the initial concentration of the target degradant and  $C_t$  was the concentration of the target degradant in the solution at time  $t$ . The degradation rate of this experiment was calculated using the following Equation (5) [29]. Additionally, H<sub>2</sub>SO<sub>4</sub> (pH = 2) and KOH (pH = 11) were employed to adjust the pH in the reaction parameter influence tests. All the experiments were carried out for three times to minimize the errors.

$$\eta\% = [(C_0 - C_t)/C_0] \times 100\% = [(C_0 - C_t)/C_0] \times 100\% = (1 - A_t/A_0) \times 100\% \quad (5)$$

### 3. Results and Discussion

#### 3.1. XRD and SEM Analysis

In order to obtain the crystallographic structure of different types of the as-prepared  $\text{MnO}_2$ , X-ray diffraction (XRD) was carried out and results were displayed in Figure 1. As depicted in Figure 1a, lines appearing at  $28.7^\circ$ ,  $37.3^\circ$ ,  $40.9^\circ$ ,  $42.8^\circ$ ,  $56.7^\circ$ ,  $59.3^\circ$ ,  $64.9^\circ$ ,  $67.3^\circ$  and  $72.3^\circ$  can be appreciably consistent with characteristic lines of  $\beta\text{-MnO}_2$  (JCPDS: 24-0735), corresponding to the (110), (101), (200), (111), (211), (220), (002), (310) and (301) planes of tetragonal  $\beta\text{-MnO}_2$  crystals [30]. Meanwhile, several diffraction lines at  $12.6^\circ$ ,  $18.0^\circ$ ,  $28.7^\circ$ ,  $37.4^\circ$ ,  $41.8^\circ$ ,  $49.7^\circ$ ,  $56.4^\circ$ ,  $59.9^\circ$ ,  $65.0^\circ$  and  $69.2^\circ$  displayed in Figure 1b can be indexed to the hexagonal phase of  $\text{K}_{1.33}\text{Mn}_8\text{O}_{16}$  (JCPDS: 77-1796) with the exposure of (110), (200), (130), (330), (240), (140), (251), (620), (002) and (541) planes. In addition, lines at  $12.7^\circ$ ,  $18.0^\circ$ ,  $25.7^\circ$ ,  $28.7^\circ$ ,  $37.5^\circ$ ,  $42.0^\circ$ ,  $49.7^\circ$ ,  $56.3^\circ$ ,  $60.0^\circ$ ,  $65.3^\circ$ ,  $69.2^\circ$  and  $72.8^\circ$  shown in Figure 1c, were attributed to (110), (200), (220), (310), (211), (301), (411), (600), (260), (002), (541) and (321) crystal facets of tetragonal  $\alpha\text{-MnO}_2$  (JCPDS: 44-0141) [31]. These phenomena could rationally verify that three types of  $\text{MnO}_2$  were supposed to be pure  $\beta\text{-MnO}_2$ , mixed  $\text{K}_{1.33}\text{Mn}_8\text{O}_{16}$  and pure  $\alpha\text{-MnO}_2$ , respectively. In addition, all three  $\text{MnO}_2$  catalysts prepared in this study exhibited an excellent crystallinity and no obvious spurious lines appeared in characteristic XRD patterns, indicating that pure  $\text{MnO}_2$  materials were successfully synthesized.

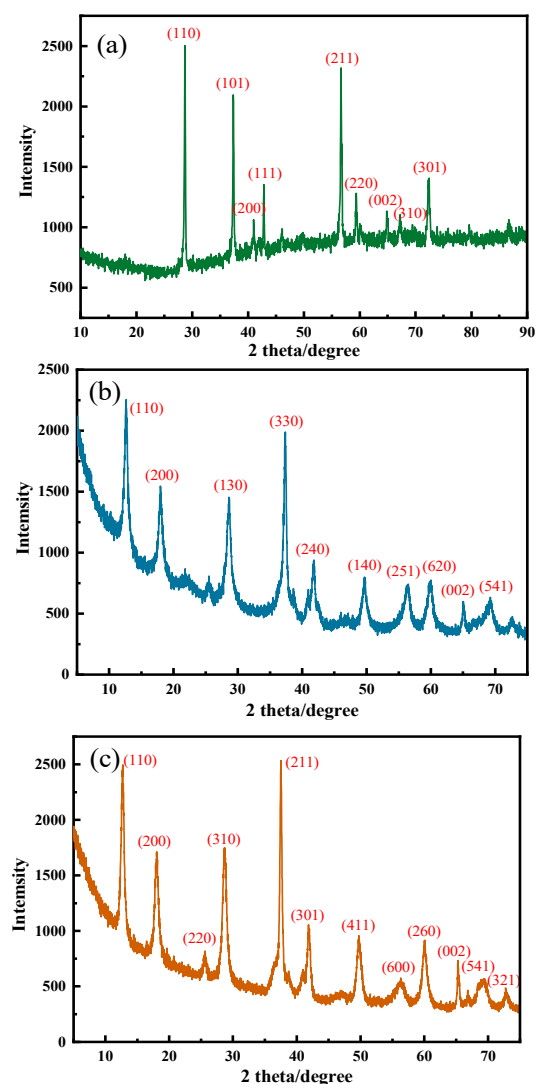
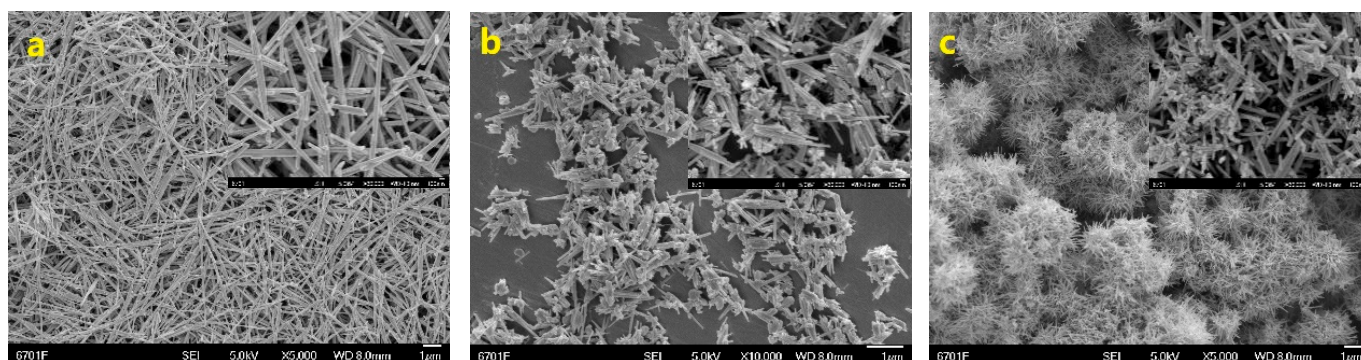


Figure 1. XRD patterns of  $\beta\text{-MnO}_2$  (a),  $\text{K}_{1.33}\text{Mn}_8\text{O}_{16}$  (b) and  $\alpha\text{-MnO}_2$  (c).

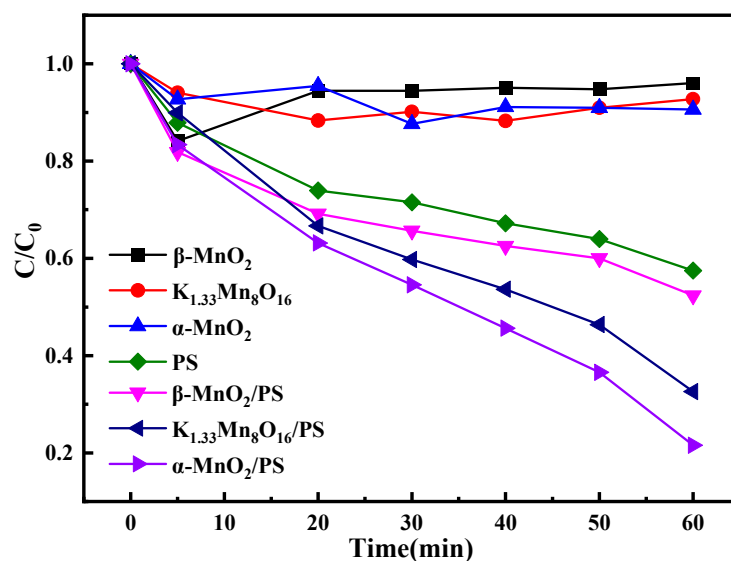
Besides, to further analyzed the surface morphology of  $\beta$ -MnO<sub>2</sub>, K<sub>1.33</sub>Mn<sub>8</sub>O<sub>16</sub> and  $\alpha$ -MnO<sub>2</sub>, SEM consequences of different samples were shown in Figure 2. As exhibited in Figure 2a, as-prepared smooth and evenly distributed rod-like  $\beta$ -MnO<sub>2</sub> with an average diameter of about 80 nm showed a number of aggregated states. Moreover, the combination between MnO<sub>2</sub> nanoparticles and MnO<sub>2</sub> nanorods observed in Figure 2b, were matched with K<sub>1.33</sub>Mn<sub>8</sub>O<sub>16</sub>, a kind of mixed MnO<sub>2</sub>. While,  $\alpha$ -MnO<sub>2</sub> displayed acicular-like appearance in Figure 2c were agglomerated with an average diameter of about 60 nm. In addition, rod-like  $\beta$ -MnO<sub>2</sub> and acicular-like  $\alpha$ -MnO<sub>2</sub> are essentially MnO<sub>2</sub> nanorods, and the mixed type is a combination one. However, the shorter length and finer diameter of  $\alpha$ -MnO<sub>2</sub> led to larger specific surface area in comparing with  $\beta$ -MnO<sub>2</sub> and K<sub>1.33</sub>Mn<sub>8</sub>O<sub>16</sub>, which could theoretically provide more reaction and activation sites to better activate PS [32]. This inference was proved by the subsequent experiments.



**Figure 2.** SEM images of  $\beta$ -MnO<sub>2</sub> (a), K<sub>1.33</sub>Mn<sub>8</sub>O<sub>16</sub> (b) and  $\alpha$ -MnO<sub>2</sub> (c).

### 3.2. Organic Pollutants Degradation Performance

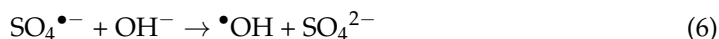
Herein, the degradation experiments of Rh B were carried out in various systems under the unadjusted pH (4.86) to evaluate and compare the organic pollutants degradation performance of three types of MnO<sub>2</sub>. As presented in Figure 3, only about 4.01%, 7.13% and 9.46% of Rh B could be removed with absorption of  $\beta$ -MnO<sub>2</sub>, K<sub>1.33</sub>Mn<sub>8</sub>O<sub>16</sub> and  $\alpha$ -MnO<sub>2</sub>, respectively, which revealed the decolorization of Rh B had little to do with adsorption. Besides, the degradation efficiency of Rh B was less than 45% over 60 min with the single PS addition, which was ascribed to the weak direct oxidation of PS ( $E_0 = 2.01$  V) [33]. This result suggested that chemical oxidation alone could not efficiently oxidized organic pollutants. Noted, for as-synthesized  $\beta$ -MnO<sub>2</sub>, K<sub>1.33</sub>Mn<sub>8</sub>O<sub>16</sub> and  $\alpha$ -MnO<sub>2</sub>, the Rh B removal efficiency was markedly improved in presence of each type of MnO<sub>2</sub> and PS simultaneously, indicated that the activation effect on PS of catalysts in aqueous solution play a vital role in the degradation of organic pollutants [34]. Among them, the efficiency of PS activation on Rh B degradation with different catalysts was  $\alpha$ -MnO<sub>2</sub> > K<sub>1.33</sub>Mn<sub>8</sub>O<sub>16</sub> >  $\beta$ -MnO<sub>2</sub>, which was 78.43%, 67.48% and 47.62%, respectively. The result was consistent with those inference obtained by SEM analysis, which was mainly caused by larger specific surface area  $\alpha$ -MnO<sub>2</sub> possessed. In detail, the specific surface area of  $\beta$ -MnO<sub>2</sub> with a rod-like structure was approximately 7.9~13.2 m<sup>2</sup>/g, which was much lower than that of  $\alpha$ -MnO<sub>2</sub> with a needle-like structure (44.4~76.5 m<sup>2</sup>/g) [32,35], while the specific surface area of hybrid MnO<sub>2</sub> should be somewhere in between. Thus,  $\alpha$ -MnO<sub>2</sub> enhanced the activation of PS with its ability to expose more active sites, facilitating the elimination of Rh B in water.



**Figure 3.** Time course of Rh B absorption and degradation via PS activation by different types of catalysts. Experiment conditions: PS concentration = 0.6 g/L, catalyst dosage = 0.8 g/L, Rh B concentration = 10 mg/L.

### 3.3. Optimization of Reaction Parameters

Generally speaking, as we all know that the addition of catalyst dosage, PS dosage and catalyst/PS dosing ratio play important roles in degradation experiments by PS activation. Moreover, detecting the influence of initial pH is great significance to prove the adaptability of  $\alpha$ -MnO<sub>2</sub> in complicated practical water with various pH in the different places [36]. Therefore, a series of tests were conducted to optimize reaction conditions. The effect of  $\alpha$ -MnO<sub>2</sub> dosage (0.2 g/L, 0.4 g/L, 0.6 g/L, 0.8 g/L and 1.2 g/L) on the Rh B degradation was displayed in Figure 4a. Obviously, the removal rate of Rh B promoted (43.38%, 62.71%, 68.89%, 78.61%, 84.49% and 93.80%) with the increased concentration of the  $\alpha$ -MnO<sub>2</sub>. Likewise, as illustrated in Figure 4b, the decoloration efficiency of Rh B promoted with the increased dosage of PS, loading from 0.2 to 1.2 g/L corresponding to degradation efficiency of 38.31%, 59.85%, 75.25%, 81.39%, 85.61% and 86.71%. These phenomena might imply that with the increase of the amount of catalyst and PS, the available active metal ions increased, which accelerated the activation of PS and generated more active substance to degrade Rh B more efficiently [28]. In consideration of economics and inhibition caused by interaction between the catalyst and PS, reasonable catalyst/PS dosing ratio needed to be determined experimentally. It can be seen from Figure 4c that when the ratio of  $\alpha$ -MnO<sub>2</sub>/PS was 2:1 (the concentration of the  $\alpha$ -MnO<sub>2</sub> and PS were 1.2 g/L and 0.6 g/L, respectively), the effect of activating PS to degrade Rh B was best. The effects of initial pH were studied at different values of 3, 5, 7, 9 and 11, as shown from Figure 4d, the degradation rate decreases significantly with the pH value increasing. 97.41% of Rh B could be removed for 60 min at the pH of 3, while the pH was increased to 5, 7, or 9, the degradation efficiency decreased by 18%, 25, or 27% over 60 min. In addition, when the pH was increased to 11, only 28.53% of Rh B was removed. The reasons of this result were as follow: (1) The zero point charge of MnO<sub>2</sub> and its complexes was reported to generally occur in the pH range of 3 to 5 [35,37,38]. Therefore, when the pH was sufficiently low, the crystalline surface became positively charged, which was more favorable for electrostatic adsorption between the electron-rich contaminants, PS and  $\alpha$ -MnO<sub>2</sub>; (2) When the pH was too high, the large amount of SO<sub>4</sub><sup>2-</sup> produced by the reactivity of SO<sub>4</sub><sup>•-</sup> and OH<sup>-</sup> (Equation (6)), caused the loss of SO<sub>4</sub><sup>•-</sup> [39].



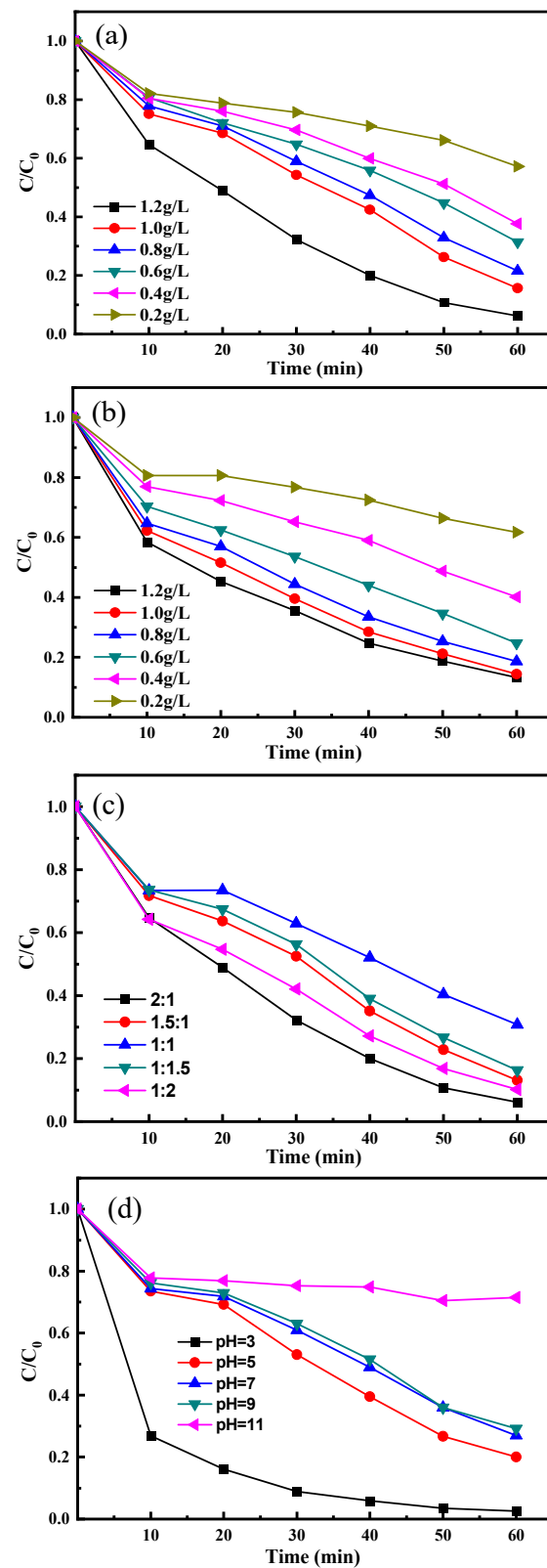


**Figure 4.** Effect of reaction parameters on the degradation of Rh B: catalyst dosage (a), persulfate concentration (b), catalyst/PS dosing ratio (c) and initial pH value (d). Experiment conditions: PS concentration = 0.6 g/L, catalyst dosage = 0.6 g/L, catalyst/PS dosing ratio = 2:1, Rh B concentration = 10 mg/L and initial pH value = 4.86 (unadjusted).

### 3.4. Mechanism Analysis

Based on the previous study [19,24,28], we proposed a possible mechanism in  $\alpha$ -MnO<sub>2</sub>/PS reaction system. As shown in Figure 5, continuous conversion of Mn (IV) and Mn (III), which occurred on the surface of  $\alpha$ -MnO<sub>2</sub> were depicted in Equations (7) and (8), a great number of SO<sub>4</sub><sup>•-</sup> produced via the activation of PS. Moreover, moiety SO<sub>4</sub><sup>•-</sup> could further react with H<sub>2</sub>O to induce  $\cdot$ OH (Equation (9)). Therefore, the mineralization of Rh B was mainly ascribed to strong active species, SRs (SO<sub>4</sub><sup>•-</sup>), hydroxyl radicals ( $\cdot$ OH) and even persulfate (PS). SO<sub>4</sub><sup>•-</sup> radicals and  $\cdot$ OH radicals would preferentially attack the central carbon ring position of Rh B to decolorize the dye and further degrade it through a ring opening process. Rh B would be converted into complex xanthene benzene radicals and produce three different forms of phthalic acid (phthalic acid, isophthalic acid and p-phthalic acid) [40]. In addition, an alternative degradation pathway for Rh B under SO<sub>4</sub><sup>•-</sup> radicals and  $\cdot$ OH radicals attacking has been proposed. The main degradation products were malonic acid, oxalic acid, glycine, m-aminophenol, adipic acid, 2-hydroxybenzoic acid and trans-crotonic acid [41], as long as they were converted to simpler organic acids and inorganic small molecule compounds by stepwise oxidation. Most of the above low molecular weight acids were environmentally friendly and may also be eventually converted to CO<sub>2</sub>, H<sub>2</sub>O and inorganic compounds.

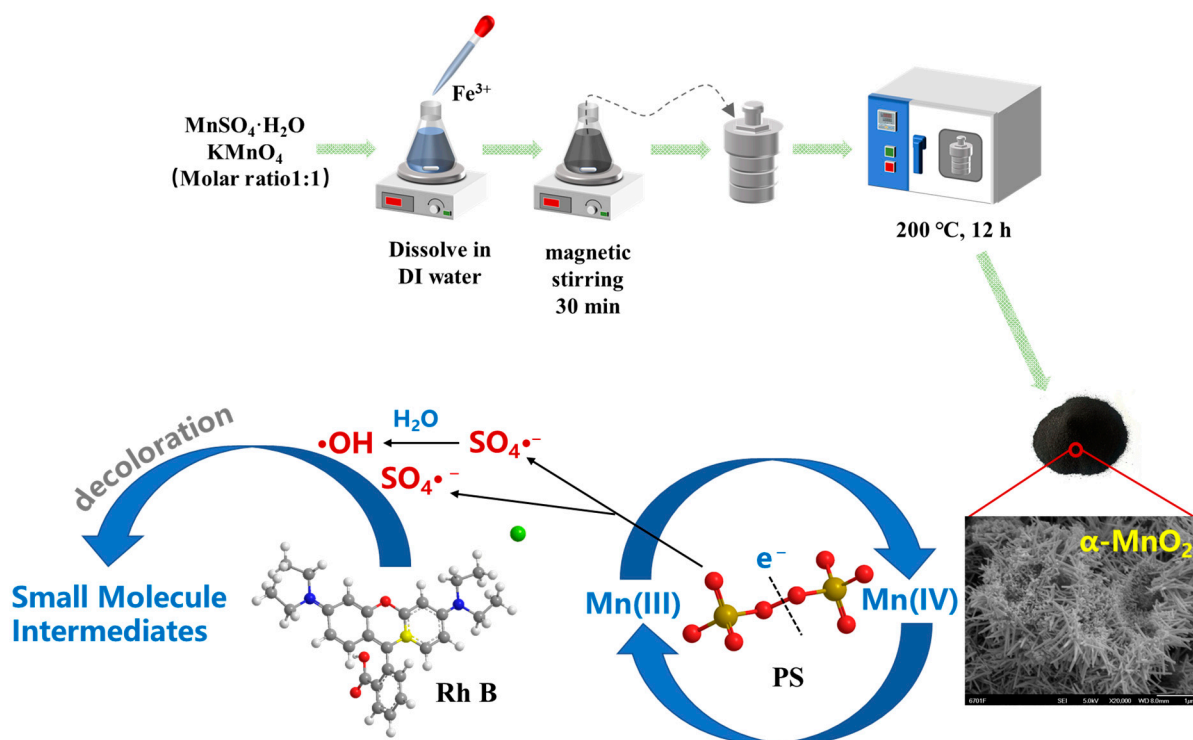
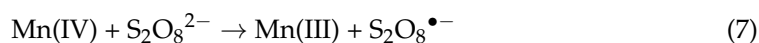


**Figure 5.** Proposed mechanism of Rh B degradation under  $\alpha$ -MnO<sub>2</sub>/PS system.

### 3.5. Reusability of $\alpha$ -MnO<sub>2</sub>

Generally speaking, stability of catalysts is one of the most important characteristics in all evaluation indicators. Considering practical application potential of  $\alpha$ -MnO<sub>2</sub>, the repeated degradation experiment was performed for four runs. As exhibited in Figure 6, the degradation efficiency got slightly decreased after each cycle, from 97.41% to 89.76%,

indicating that  $\alpha$ -MnO<sub>2</sub> had expectation of putting into practical application in the organic pollutants' degradation due to its good repeatability. In addition, there were several reasons could explain this reduction of removal rate along the Rh B recycle degradation: (1) the slight leaching of metal ions on the catalyst [42,43]; (2) the absorption of degradation intermediate or remaining Rh B occupied the active sites on the surface of the catalyst in the previous cycle [43]; (3) the by-production produced during the several cycles would compete for active species with the Rh B molecules [44].

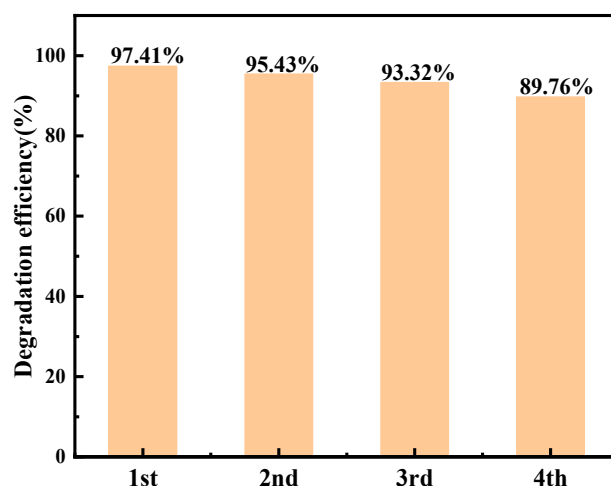


**Figure 6.** Performance of  $\alpha$ -MnO<sub>2</sub> upon 4 successive uses for Rh B degradation. Experimental conditions: PS concentration = 0.6 g/L, catalyst dosage = 1.2 g/L, Rh B concentration = 10 mg/L.

#### 4. Conclusions

All in all, rod-shaped, acicular and mixed MnO<sub>2</sub> were successfully fabricated by hydrothermal method with controlling the conditions of reaction and addition of the metal ions. From the results of surface morphology and crystallographic structure analyzed by scanning electron microscope (SEM) and X-ray diffraction (XRD), three different morphologies of MnO<sub>2</sub> were corresponding to  $\beta$ -MnO<sub>2</sub>, mixed K<sub>1.33</sub>Mn<sub>8</sub>O<sub>16</sub> and  $\alpha$ -MnO<sub>2</sub>, respectively. In the microscopic state, the  $\alpha$ -MnO<sub>2</sub> nanorods were more dispersed, and their nanorods were shorter in length and smaller in diameter. The mixed type, K<sub>1.33</sub>Mn<sub>8</sub>O<sub>16</sub> was a combination of manganese dioxide nanorods and manganese dioxide particles. In contrast, the  $\beta$ -MnO<sub>2</sub> mostly showed a polymerized state. Thus, the  $\alpha$ -MnO<sub>2</sub> with needle-shaped microscopic morphology had a larger specific surface area and could provide more activation sites. As-prepared  $\alpha$ -MnO<sub>2</sub> had a superior activity for Rh B degradation with the addition of PS, and 97.41% of Rh B could be removed within 60 min. More importantly, the reaction parameters are also optimized in this study, when the catalyst/PS ratio was 2:1 (the concentration of the  $\alpha$ -MnO<sub>2</sub> and PS were 1.2 g/L and 0.6 g/L, respectively), pH value was 3, and the best catalytic efficiency for PS activation was obtained at the temperature of 20 °C. Meanwhile, the probable degradation mechanism was also proposed. What's more, the catalyst was reused 4 times, and the degradation rate decreased by less than 10%. In a word, this study provided an important reference for study on activation of PS by manganese oxides and their multicomponent complexes and exploitation of new nano materials for efficient removal of organic dyes in wastewater. In future research, the preparation of composite materials from  $\alpha$ -MnO<sub>2</sub> with needle-shaped microscopic morphology together with other substances as raw materials could be explored in depth. For example, magnetic composites can be prepared to facilitate the recovery of the catalyst. Or other reactants can be added to obtain composites with better activation and regeneration performance.

**Author Contributions:** X.Z. contributed to the Data curation, writing—original draft preparation, X.G. and S.C. contributed to the writing—review and editing; J.S. and X.C. contributed to the supervision, funding acquisition. All authors have read and agreed to the published version of the manuscript.

**Funding:** This research received no external funding.

**Data Availability Statement:** Data available in a publicly accessible repository.

**Acknowledgments:** This work was supported by Research and Innovation Team Cultivation Program of Yili Normal University (CXZK2021004) and Natural Science Foundation of Xinjiang Uygur Autonomous Region (2021D01C461).

**Conflicts of Interest:** The authors declare no conflict of interest.

## References

1. Zhang, X.; Wang, J.; Dong, X.-X.; Lv, Y.-K. Functionalized metal-organic frameworks for photocatalytic degradation of organic pollutants in environment. *Chemosphere* **2020**, *242*, 125144. [[CrossRef](#)] [[PubMed](#)]
2. Zhang, W.; Tay, H.L.; Lim, S.S.; Wang, Y.; Zhong, Z.; Xu, R. Supported cobalt oxide on MgO: Highly efficient catalysts for degradation of organic dyes in dilute solutions. *Appl. Catal. B Environ.* **2010**, *95*, 93–99. [[CrossRef](#)]
3. Guo, N.; Liu, H.; Fu, Y.; Hu, J. Preparation of Fe<sub>2</sub>O<sub>3</sub> nanoparticles doped with In<sub>2</sub>O<sub>3</sub> and photocatalytic degradation property for rhodamine B. *Optik* **2020**, *201*, 163537. [[CrossRef](#)]
4. Ji, R.; Zhao, Z.; Yu, X.; Chen, M. Determination of rhodamine B in capsicol using the first derivative absorption spectrum. *Optik* **2019**, *181*, 796–801. [[CrossRef](#)]
5. Pearce, C., Jr.; Lloyd, J.; Guthrie, J. The removal of colour from textile wastewater using whole bacterial cells: A review. *Dye. Pigment.* **2003**, *58*, 179–196. [[CrossRef](#)]
6. Banat, I.M.; Nigam, P.; Singh, D.; Marchant, R. Microbial decolorization of textile-dyecontaining effluents: A review. *Bioresour. Technol.* **1996**, *58*, 217–227. [[CrossRef](#)]
7. Foti, L.; Coviello, D.; Zuurro, A.; Lelario, F.; Bufo, S.A.; Scranò, L.; Sauvetre, A.; Chiron, S.; Brienza, M. Comparison of Sunlight-Aops for Levofloxacin Removal: Kinetics, Transformation Products, and Toxicity Assay on Escherichia Coli and Micrococcus Flavus. *Environ. Sci. Pollut. Res.* **2022**, *29*, 58201–58211. [[CrossRef](#)]
8. Ennouri, R.; Lavecchia, R.; Zuurro, A.; Elaoud, S.C.; Petrucci, E. Degradation of chloramphenicol in water by oxidation on a boron-doped diamond electrode under UV irradiation. *J. Water Process. Eng.* **2021**, *41*, 101995. [[CrossRef](#)]
9. Huixuan, Z.; Nengzi, L.-C.; Wang, Z.; Zhang, X.; Li, B.; Cheng, X. Construction of Bi<sub>2</sub>O<sub>3</sub>/Cunife Ldhs Composite and Its Enhanced Photocatalytic Degradation of Lomefloxacin with Persulfate under Simulated Sunlight. *J. Hazard. Mater.* **2020**, *383*, 121236.
10. Pirsahab, M.; Hossaini, H.; Janjani, H. Reclamation of hospital secondary treatment effluent by sulfate radicals based-advanced oxidation processes (SR-AOPs) for removal of antibiotics. *Microchem. J.* **2019**, *153*, 104430. [[CrossRef](#)]
11. Lei, Z.; Yang, X.; Ji, Y.; Wei, J. Sulfate Radical-Based Oxidation of the Antibiotics Sulfamethoxazole, Sulfisoxazole, Sulfathiazole, and Sulfamethizole: The Role of Five-Membered Heterocyclic Rings. *Sci. Total Environ.* **2019**, *692*, 201–208.
12. Chen, C.; Feng, H.; Deng, Y. Re-evaluation of sulfate radical based-advanced oxidation processes (SR-AOPs) for treatment of raw municipal landfill leachate. *Water Res.* **2019**, *153*, 100–107. [[CrossRef](#)] [[PubMed](#)]
13. Wang, J.; Wang, S. Activation of persulfate (PS) and peroxymonosulfate (PMS) and application for the degradation of emerging contaminants. *Chem. Eng. J.* **2018**, *334*, 1502–1517. [[CrossRef](#)]
14. Yang, L.; He, L.; Xue, J.; Ma, Y.; Xie, Z.; Wu, L.; Huang, M.; Zhang, Z. Persulfate-based degradation of perfluorooctanoic acid (PFOA) and perfluorooctane sulfonate (PFOS) in aqueous solution: Review on influences, mechanisms and prospective. *J. Hazard. Mater.* **2020**, *393*, 122405. [[CrossRef](#)]
15. Matzek, L.W.; Carter, K.E. Activated persulfate for organic chemical degradation: A review. *Chemosphere* **2016**, *151*, 178–188. [[CrossRef](#)]
16. Zhang, M.; Chen, X.; Zhou, H.; Murugananthan, M.; Zhang, Y. Degradation of p-nitrophenol by heat and metal ions co-activated persulfate. *Chem. Eng. J.* **2015**, *264*, 39–47. [[CrossRef](#)]
17. Ruonan, G.; Meng, Q.; Zhang, H.; Zhang, X.; Li, B.; Cheng, Q.; Cheng, X. Construction of Fe<sub>2</sub>O<sub>3</sub>/Co<sub>3</sub>O<sub>4</sub>/Exfoliated Graphite Composite and Its High Efficient Treatment of Landfill Leachate by Activation of Potassium Persulfate. *Chem. Eng. J.* **2019**, *355*, 952–962.
18. Xing, S.; Li, W.; Liu, B.; Wu, Y.; Gao, Y. Removal of Ciprofloxacin by Persulfate Activation with CuO: A Ph-Dependent Mechanism. *Chem. Eng. J.* **2020**, *382*, 122837. [[CrossRef](#)]
19. Junjing, L.; Guo, R.; Ma, Q.; Nengzi, L.-C.; Cheng, X. Efficient Removal of Organic Contaminant via Activation of Potassium Persulfate by  $\Gamma$ -Fe<sub>2</sub>O<sub>3</sub>/A-MnO<sub>2</sub> Nanocomposite. *Sep. Purif. Technol.* **2019**, *227*, 115669.
20. Miao, L.; Wang, J.; Zhang, P. Review on manganese dioxide for catalytic oxidation of airborne formaldehyde. *Appl. Surf. Sci.* **2019**, *466*, 441–453. [[CrossRef](#)]
21. Wang, Y.; Chen, S. Droplets impact on textured surfaces: Mesoscopic simulation of spreading dynamics. *Appl. Surf. Sci.* **2015**, *327*, 159–167. [[CrossRef](#)]

22. Ning, S.; Duan, Y.; Jiao, X.; Chen, D. Large-Scale Preparation and Catalytic Properties of One-Dimensional A/B-MnO<sub>2</sub> Nanostructures. *J. Phys. Chem. C* **2009**, *113*, 8560–8565.
23. Xu, Y.; Lin, H.; Li, Y.; Zhang, H. The mechanism and efficiency of MnO<sub>2</sub> activated persulfate process coupled with electrolysis. *Sci. Total. Environ.* **2017**, *609*, 644–654. [[CrossRef](#)]
24. Zhengyu, D.; Zhang, Q.; Chen, B.-Y.; Hong, J. Oxidation of Bisphenol a by Persulfate via Fe<sub>3</sub>O<sub>4</sub>-A-MnO<sub>2</sub> Nanoflower-Like Catalyst: Mechanism and Efficiency. *Chem. Eng. J.* **2019**, *357*, 337–347.
25. Deshan, Z.; Sun, S.; Fan, W.; Yu, H.; Fan, C.; Cao, G.; Yin, Z.; Song, X. One-Step Preparation of Single-Crystalline B-MnO<sub>2</sub> Nanotubes. *J. Phys. Chem. B* **2005**, *109*, 16439–16443.
26. Subramanian, V.; Zhu, H.; Vajtai, R.; Ajayan, P.M.; Wei, B. Hydrothermal Synthesis and Pseudocapacitance Properties of MnO<sub>2</sub> Nanostructures. *J. Phys. Chem. B* **2005**, *109*, 20207–20214. [[CrossRef](#)] [[PubMed](#)]
27. Jiechao, G.; Zhuo, L.; Yang, F.; Tang, B.; Wu, L.; Tung, C. One-Dimensional Hierarchical Layered K<sub>X</sub>MnO<sub>2</sub> (X < 0.3) Nanoarchitectures: Synthesis, Characterization, and Their Magnetic Properties. *J. Phys. Chem. B* **2006**, *110*, 17854–17859.
28. Gong, C.; Zhang, X.; Gao, Y.; Zhu, G.; Cheng, Q.; Cheng, X. Novel Magnetic MnO<sub>2</sub> /MnFe<sub>2</sub>O<sub>4</sub> Nanocomposite as a Heterogeneous Catalyst for Activation of Peroxymonosulfate (Pms) toward Oxidation of Organic Pollutants. *Sep. Purif. Technol.* **2019**, *213*, 456–464.
29. Lavecchia, R.; Pugliese, A.; Zuurro, A. Removal of lead from aqueous solutions by spent tea leaves. *Chem. Eng. Trans.* **2010**, *19*, 73–78.
30. Jain, N.; Roy, A. Phase & morphology engineered surface reducibility of MnO<sub>2</sub> nano-heterostructures: Implications on catalytic activity towards CO oxidation. *Mater. Res. Bull.* **2019**, *121*, 110615.
31. Rao, T.P.; Kumar, A.; Naik, V.M.; Naik, R. Effect of Carbon Nanofibers on Electrode Performance of Symmetric Supercapacitors with Composite A-MnO<sub>2</sub> Nanorods. *J. Alloys Compd.* **2019**, *789*, 518–527. [[CrossRef](#)]
32. Yang, W.; Su, Z.; Xu, Z.; Yang, W.; Peng, Y.; Li, J. Comparative Study of A-, B-, Γ- and Δ-MnO<sub>2</sub> on Toluene Oxidation: Oxygen Vacancies and Reaction Intermediates. *Appl. Catal. B Environ.* **2020**, *260*, 118150. [[CrossRef](#)]
33. Ma, Q.; Zhang, H.; Zhang, X.; Li, B.; Guo, R.; Cheng, Q.; Cheng, X. Synthesis of magnetic CuO/MnFe<sub>2</sub>O<sub>4</sub> nanocomposite and its high activity for degradation of levofloxacin by activation of persulfate. *Chem. Eng. J.* **2018**, *360*, 848–860. [[CrossRef](#)]
34. Huixuan, Z.; Song, Y.; Nengzi, L.-c.; Gou, J.; Li, B.; Cheng, X. Activation of Persulfate by a Novel Magnetic CuFe<sub>2</sub>O<sub>4</sub>/Bi<sub>2</sub>O<sub>3</sub> Composite for Lomefloxacin Degradation. *Chem. Eng. J.* **2020**, *379*, 122362.
35. Zeming, W.; Wang, Z.; Li, W.; Lan, Y.; Chen, C. Performance Comparison and Mechanism Investigation of Co<sub>3</sub>O<sub>4</sub>-Modified Different Crystallographic MnO<sub>2</sub> (A, B, Γ, and Δ) as an Activator of Peroxymonosulfate (Pms) for Sulfisoxazole Degradation. *Chem. Eng. J.* **2022**, *427*, 130888.
36. Gong, C.; Nengzi, L.-C.; Gao, Y.; Zhu, G.; Gou, J.; Cheng, X. Degradation of Tartrazine by Peroxymonosulfate through Magnetic Fe<sub>2</sub>O<sub>3</sub>/Mn<sub>2</sub>O<sub>3</sub> Composites Activation. *Chin. Chem. Lett.* **2020**, *31*, 2730–2736.
37. Hirakendu, B.; Singh, S.; Venkatesh, M.; Pimple, M.V.; Singhal, R.K. Graphene Oxide-MnO<sub>2</sub>-Goethite Microsphere Impregnated Alginate: A Novel Hybrid Nanosorbent for as (Iii) and as (V) Removal from Groundwater. *J. Water Process Eng.* **2021**, *42*, 102129.
38. Shijun, Z.; Li, H.; Wang, L.; Cai, Z.; Wang, Q.; Shen, S.; Li, X.; Deng, J. Oxygen Vacancies-Rich A@Δ-MnO<sub>2</sub> Mediated Activation of Peroxymonosulfate for the Degradation of Cip: The Role of Electron Transfer Process on the Surface. *Chem. Eng. J.* **2023**, *458*, 141415.
39. Lin, X.; Ma, Y.; Wan, J.; Wang, Y.; Li, Y. Efficient degradation of Orange G with persulfate activated by recyclable FeMoO<sub>4</sub>. *Chemosphere* **2019**, *214*, 642–650. [[CrossRef](#)]
40. Meng, F.; Song, M.; Song, B.; Wei, Y.; Cao, Q.; Cao, Y. Enhanced degradation of Rhodamine B via α-Fe<sub>2</sub>O<sub>3</sub> microspheres induced persulfate to generate reactive oxidizing species. *Chemosphere* **2019**, *243*, 125322. [[CrossRef](#)]
41. Moutusi, D.; Bhattacharyya, K.G. Oxidation of Rhodamine B in Aqueous Medium in Ambient Conditions with Raw and Acid-Activated MnO<sub>2</sub>, NiO, ZnO as Catalysts. *J. Mol. Catal. A Chem.* **2014**, *391*, 121–129.
42. Huixuan, Z.; Wang, J.; Zhang, X.; Li, B.; Cheng, X. Enhanced Removal of Lomefloxacin Based on Peroxymonosulfate Activation by Co<sub>3</sub>O<sub>4</sub>/Δ-FeOOH Composite. *Chem. Eng. J.* **2019**, *369*, 834–844.
43. Zhongjuan, W.; Nengzi, L.-C.; Zhang, X.; Zhao, Z.; Cheng, X. Novel NiCo<sub>2</sub>S<sub>4</sub>/Cs Membranes as Efficient Catalysts for Activating Persulfate and Its High Activity for Degradation of Nimesulide. *Chem. Eng. J.* **2020**, *381*, 122517.
44. Huixuan, Z.; Nengzi, L.-C.; Li, X.; Wang, Z.; Li, B.; Liu, L.; Cheng, X. Construction of CuBi<sub>2</sub>O<sub>4</sub>/MnO<sub>2</sub> Composite as Z-Scheme Photoactivator of Peroxymonosulfate for Degradation of Antibiotics. *Chem. Eng. J.* **2020**, *386*, 124011.

**Disclaimer/Publisher's Note:** The statements, opinions and data contained in all publications are solely those of the individual author(s) and contributor(s) and not of MDPI and/or the editor(s). MDPI and/or the editor(s) disclaim responsibility for any injury to people or property resulting from any ideas, methods, instructions or products referred to in the content.